Estimation of degraded composite laminate properties using acoustic wave propagation model and a reduction-prediction network

D. Roy Mahapatra, S. Suresh, S.N. Omkar and S. Gopalakrishnan
Department of Aerospace Engineering, Indian Institute of Science, Bangalore, India

Received April 2004
Revised February 2005
Accepted March 2005

Abstract

Purpose – To develop a new method for estimation of damage configuration in composite laminate structure using acoustic wave propagation signal and a reduction-prediction neural network to deal with high dimensional spectral data.

Design/methodology/approach – A reduction-prediction network, which is a combination of an independent component analysis (ICA) and a multi-layer perceptron (MLP) neural network, is proposed to quantify the damage state related to transverse matrix cracking in composite laminates using acoustic wave propagation model. Given the Fourier spectral response of the damaged structure under frequency band-selective excitation, the problem is posed as a parameter estimation problem. The parameters are the stiffness degradation factors, location and approximate size of the stiffness-degraded zone. A micro-mechanics model based on damage evolution criteria is incorporated in a spectral finite element model (SFEM) for beam type structure to study the effect of transverse matrix crack density on the acoustic wave response. Spectral data generated by using this model is used in training and testing the network. The ICA network called as the reduction network, reduces the dimensionality of the broad-band spectral data for training and testing and sends its output as input to the MLP network. The MLP network, in turn, predicts the damage parameters.

Findings – Numerical demonstration shows that the developed network can efficiently handle high dimensional spectral data and estimate the damage state, damage location and size accurately.

Research limitations/implications – Only numerical validation based on a damage model is reported in absence of experimental data. Uncertainties during actual online health monitoring may produce errors in the network output. Fault-tolerance issues are not attempted. The method needs to be tested using measured spectral data using multiple sensors and wide variety of damages.

Practical implications – The developed network and estimation methodology can be employed in practical structural monitoring system, such as for monitoring critical composite structure components in aircrafts, spacecrafts and marine vehicles.

Originality/value – A new method is reported in the paper, which employs the previous works of the authors on SFEM and neural network. The paper addresses the important problem of high data dimensionality, which is of significant importance from practical engineering application viewpoint.

Keywords Acoustic waves, Finite element analysis, Neural nets, Laminates, Estimation

Paper type Technical paper

Engineering Computations: International Journal for Computer-Aided Engineering and Software
Vol. 22 No. 7, 2005
pp. 849-876

0264-4401
DOI 10.1108/02644400510619558

1. Introduction

Online structural health monitoring (SHM) of composite structures using embedded acoustic devices and wave-based diagnostic strategies is becoming an affordable technology and is expected to reduce the time and cost spent on the ground-based non-destructive evaluation (NDE). Subsequently, such SHM systems may provide a much better management of the operational life of the structure, particularly components of aerospace vehicles which are crucial to their performance and survivability. Before the hardware (sensors, actuators, networks, processors and data storage devices) and the integrated platform for operation of such system (often discussed using terminologies like sensor fusion, data fusion, etc.) can take shape, a significant amount of effort appears necessary in developing SHM software and algorithms at various levels of complexity.

The existence of a damage or structural degradation is generally traced by comparing the time-domain travelling wave response of the structure at the current state with a base-line response. Any fluctuation in the response can be correlated to the damage/degradation location through the arrival-time of the new peaks (scattered wave). This is also true for damage initiation and progression in the form of strain energy release from the damaged zone that arrives at the measurement location in the form of stress waves. Apart from purely experimental techniques based on such idea, which are common in NDE, vibration-based techniques involving finite element updated models followed by certain post-processing strategies can also provide gross location of the damage. Such techniques based on finite element models of healthy structures and post-processing of measured data involve either:

- extraction of component modal information such as change in natural frequencies, strain mode shape, etc. (Doebling *et al.*, 1996; Ratcliffe, 2000) or
- estimation of certain damage indicator (Schulz *et al.*, 1998; Zhang *et al.*, 1999; Nag *et al.*, 2002a) capable of directly locating the existence and gross location of the damage.

However, such component modal information and the damage indicators are found to be useful in predicting only the gross location or size of the damage, when they are large. On the other hand, while using broad-band acoustic signal for interrogating smaller size of damage, the above methods fail to capture all the damage parameters (certain stiffness degradation factors, location as well as the size), simultaneously.

Identification of the size of damaged/degraded zone in composite and its type, i.e. matrix cracking, splitting, delamination, fiber fracture, thermal damage or combination of any of these, falls in the category of inverse problem. In addition, when the objective is also to estimate the stiffness degradation factors, the problem becomes much more complex. As the first step towards solving such inverse problem using soft-computing tool, such as artificial neural network (ANN), one preferably needs appropriate computational model for various types of damage in composite. Several of such model can be found in reported literature (Han and Hahn, 1989; Frantziskonis and Joshi, 1990; Frantziskonis and Desai, 1991; Joshi and Frantziskonis, 1991; Hackett and Kerry, 1992; Ogihara and Takeda, 1995; Luo-Yu, 1994, 1996; Zhang and Herrmann, 1999; Kashtalyan and Soutis, 2000; Gerald, 2000; Caiazzo and Costanzo, 2002). Many of these models have been validated using experimental results. These models can be classified as:

- interfacial shear-lag based model; and
- micro-mechanics model based on suitable damage evolution criteria.

While employing an acoustic wave interrogation technique, often it appears advantageous to use excitation signal having multiple frequency bands or single broad-band while performing diagnostic analysis of structure with damage/degradation. The idea here is to extract more hidden information from multivariate data which are sampled over more than a single and narrow frequency band (Manson *et al.*, 2003). This can lead to improved efficiency of the method for estimating multiple damage/degradation parameters. Therefore, in order to estimate the damage parameters, the computational model involving finite elements of the damaged zone must be efficient for low as well as high frequency analysis. Such a computational model is not available in reported literature.

Since the objective is to solve an inverse problem, an estimator with statistical feature, such as ANN (Darmala *et al.*, 1992; Wu *et al.*, 1992; Song and Schmerr, 1992; Rhim and Lee, 1995; Zgonc and Achenbach, 1996; Chang *et al.*, 2000; Sung *et al.*, 2000; Ishak *et al.*, 2001; Liu *et al.*, 2002) can be found suitable. However, most of these studies deal with estimation of either the stiffness degradation or the location/size of the damage. Simultaneous prediction of the in-plane, bending and shear stiffness degradations, the location and the size of the degraded zone has not been addressed in any of the reported methods and studies.

Recently, in the works of Garg *et al.* (2004), an efficient spectral finite element-based estimation strategy using multi-layer perceptron (MLP) network has been developed, where one can use acoustic wave response (over a specified frequency band) of the degraded laminated composite structure to train the network. The reliability of estimating the location and quantifying the state of ply degradation was studied in that work. The network was trained for a specific spectral band with a prescribed resolution. Such strategy involves retraining the network, when a different spectral band is to be used. In the present paper we improve upon the previous method by developing a reduction-prediction network, which employs the broad-band spectral data using spectral finite element model (SFEM) for simultaneous prediction of the in-plane, bending, shear stiffness degradations, the location as well as the size of the degraded zone. The main advantage of the proposed network architecture is that it can be employed while using any spectral resolution without retraining the network. Two important and practical aspects are addressed, which are:

(1) the use of a micro-mechanics model for matrix-cracks while simulating the acoustic wave response using spectral finite element; and

(2) the reduction-prediction network to deal with broad-band and high resolution spectral data.

Below we give a brief overview of these two aspects.

1.1 Micro-mechanics models for matrix cracks

Damage states in composite and their evolution are complex and depend on geometrical scale and properties of the material systems at the interfaces. At microscopic scale, the matrix phase of the composite shows matrix cracks, which are generally characterized by matrix crack density. In laminated composite, such matrix

cracks appear due to fiber separation in angle plies (mainly 90° plies in cross-ply laminates). Under in-plane tensile load, as well as under bending load, these transverse matrix cracks first grow through the thickness of the layer and reach the top and the bottom interfaces with the neighbouring layers. They also increase in number under increasing deformation. Owing to mismatch in the elastic moduli between the neighbouring layers, there exists an on-set of delamination, and beyond some critical value of the strain energy release rate, the delaminations start growing rapidly. As a result, under the condition that transverse matrix crack density is very high and that the angle plies can no longer take tensile load, all the tensile load is transferred through the 0° fibers, and they break, which is the final stage of failure. Under compressive load also, the laminates start buckling at the delaminated zone and may fail instantaneously. The evolution of matrix crack as the initial stage of damage followed by delamination is also true for composite subjected to impact load (Choi *et al.*, 1991a, b; Liu *et al.*, 1993). In most of the reported damage models for transverse matrix cracks, splitting, delamination, etc. and combination of them, the laminate stiffness degradation can be used as the effective damage parameters. Aveston and Kelly (1973) along with Hahn and Tsai (1974) were among the first researchers to account for stiffness degradation due to matrix cracks in advanced composite. Subsequently, more consistent models with less assumptions have been proposed. However, all these majority of the methods for prediction of the reduced properties of cracked laminates are applicable only to cross-ply laminates. A detail review on these models can be found in Abrate (1991). More consistent and general models, which are applicable for general ply stacking and combined bending and extensional loading were developed. These consistent models are based on certain damage evolution criteria. Since such a criteria needs calculation of the stresses and strains in the vicinity of the cracks during initiation and progression, it appears advantageous to combine a model-based stress-strain prediction technique with the calculation of appropriate damage evolution function such as the strain energy release rate. One of such general model with experimental data were reported by Adolfsson and Gudmundson (1997, 1999). Similar model based on Helmoltz free energy as a damage evolution function and a homogenization technique was used by Caiazzo and Costanzo (2001) to estimate the macroscopic constitutive behaviour. In the present paper, we incorporate the model of Adolfsson and Gudmundson (1997) in a SFEM for acoustic wave propagation analysis. We propose a reduction-prediction network, in which one independent component analysis (ICA) network performs the dimensionality reduction of the spectral data. The output of this ICA network is fed as input to one MLP feed forward network for estimation of the damage parameters. Once estimated, such damage parameters can further be correlated to the damage states. A detail review on the various available models for stiffness degradation due to surface-breaking transverse crack, transverse matrix cracks and delamination in laminated composite have been discussed by Garg *et al.* (2004). Before developing the reduction-prediction network, we first simulate the nature of wave scattering and the effect of change in the matrix crack density on the acoustic wave response.

1.2 Dimensionality reduction

The second aspect associated with the spectral estimation problem is the large size of spectral data, especially when the measurement is carried out over multiple frequency

bands with high resolution. In our present problem, this spectral data are complex-valued Fourier spectrum of displacements at certain span-wise location of a laminated composite beam. The range of target measurement frequencies and complying with it, the frequency band used in the chosen model for generation of ANN training data, may vary from few kHz to MHz. In the present paper, we shall typically consider the frequency sampling $\Delta\omega_n$ in the range of 10-50 Hz over the wide band. There is one additional problem with such data while employing ANN. In other words, if the complex-valued spectrum of displacements/strains (or their rates, etc.) at fixed frequency sampling is used for training of an ANN, then the testing as well as the real-time use of that ANN must be carried out using the data acquired at same frequency sampling. This type of ANN eliminates the scope of using a varying frequency sampling, and in effect, eliminates the scope of real-time tunning of the network performance. Also, there may be other factors, such as significant redundancy in the feature space of the data sets used during the ANN training. If such redundancy is avoided, then the computational cost of training the ANN can be reduced to a greater extent. Hence the overall problem is two-fold. First is the mapping of the acquired spectral data, whatever frequency sampling they have, into a non-redundant data of fixed size. Second is the approximating the relationship between the non-redundant data and the damage parameters. Transformation of the redundant spectral data into the non-redundant data, which leads to dimensionality reduction, is performed in the present work using ICA (Hyvarinen, 1999) network, which is called the reduction network. The damage parameters are predicted by solving the inverse problem using the MLP network.

2. Degradation of composite laminate properties due to transverse matrix cracks

Adolfsson and Gudmundson (1997) developed a model to calculate the reduced thermoelastic properties under extension and bending for composite laminates containing matrix cracks on the basis of the decrease in elastic energy due to damage. Later, this model was used by Adolfsson and Gudmundson (1999) to develop a self-consistent damage evolution model based on strain energy release rate as the damage evolution controlling parameter. Results using this model matched well with the experimental results. The effect of interaction between a damaged cross-ply and its neighbouring 0° ply is automatically included in the formulation. Matrix cracks of arbitrary size and geometry can also be accommodated in this model. However, if it is the initiation and growth of delamination following progressive matrix cracking, then it can be modelled more efficiently using shear-lag based constrained model reported by Ogihara and Takeda (1995). In the present paper we use the damage evolution model reported by Adolfsson and Gudmundson (1997) to arrive at the constitutive model of the cracked laminates assuming that the damage state is not varying with time during acoustic wave scattering, i.e. the damage growth is not affected by the small amplitude wave propagation. Below we give a brief overview of this model. The original formulation is given in the works of Adolfsson and Gudmundson (1997, 1999) and is not repeated here.

The damage state in the kth laminate (Figure 1) is defined by the crack density d_k, where

$$d_k = \frac{t_k}{l_k}. \tag{1}$$

The load deformation relation for a single orthotropic laminate under plane strain condition (when the transverse cracks are in the form of tunnelling cracks normal to the *XZ* plane along with appropriate loading) or otherwise under plane stress condition can be expressed as

$$\begin{Bmatrix} \mathbf{N} \\ \mathbf{M} \\ \mathbf{V} \end{Bmatrix} = \begin{bmatrix} \mathbf{C}_{EE} & \mathbf{C}_{EB} & 0 \\ \mathbf{C}_{EB} & \mathbf{C}_{BB} & 0 \\ 0 & 0 & \mathbf{C}_{SS} \end{bmatrix} \begin{Bmatrix} \varepsilon_E \\ \kappa \\ \gamma_S \end{Bmatrix}, \tag{2}$$

where ε_E, κ and γ_S are, respectively, the strain vectors due to in-plane deformation, curvature and transverse shear deformation. **N**, **M** and **V** are, respectively, the vectors of in-plane forces, bending moments and transverse shear forces per unit width. The subscripts E and B associated with the strains and the stiffness coefficients, respectively, stand for extension and bending. For uncracked laminates, the elastic coefficients are functions of the Young's modulus, Poisson's ratio, fibre angle and laminate thickness only. We exclude the thermoelastic part associated with the original formulation reported by Adolfsson and Gudmundson (1997). The next steps to arrive at the change in the stiffness coefficients are as follows. The total strain energy due to the cracked laminate is expressed in following two forms.

(1) The elastic strain energy of the uncracked laminate minus the energy released due to formation of the crack surfaces (ΔW), which is given by

$$\begin{aligned} W_{(c)} &= \frac{1}{2}(\varepsilon^T \mathbf{C}\varepsilon - \Delta W) + \sum_{k=1}^{M} f_k(\sigma_{k(R)}), \\ \Delta W &= \sum_{k=1}^{M}\sum_{l=1}^{M} \sqrt{t_k d_k t_l d_l}(\sigma_k)^T \beta^{kl} \sigma_l, \end{aligned} \tag{3}$$

where $\sigma_{k(R)}$ is the residual stress, f_k is the strain energy due to interlaminar constraints and β^{kl} are the parameters to be estimated.

(2) The elastic strain energy of the cracked laminate using the degraded stiffness coefficients ($\mathbf{C}_{(c)}$) and the eigen strains ($\varepsilon^{(R)}$) due to residual stresses, which is given by

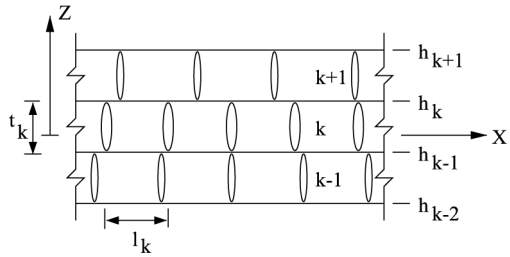

Note: The damage state of the *k*th laminate is determined by the crack density $d_k = t_k/l_k$

Figure 1.
Schematic diagram showing the laminated composite ply with transverse cracks

$$W_{(c)} = \frac{1}{2}(\boldsymbol{\varepsilon} - \boldsymbol{\varepsilon}^{(R)})^T \mathbf{C}_{(c)}(\boldsymbol{\varepsilon} - \boldsymbol{\varepsilon}^{(R)}) + \sum_{k=1}^{M} f_k(\sigma_{k(R)}). \tag{4}$$

Equating these two forms leads to a parameter estimation problem, where the stiffness coefficients of the cracked laminate as a function of these parameters (β^{kl}) are estimated in terms of the elastic coefficients of the uncracked laminate (**C**), laminate thickness, crack density, crack surface geometry and the stress intensity factors under mode-I (opening), mode-II (shearing) and mode-III (tearing/anti-plane) loading. Here, the damage evolution criteria involving these quantities is expressed with the help of the strain energy release rates ($\mathbf{G}_k$) as the damage evolution controlling parameter, and is given by

$$\begin{gathered} \mathrm{d}d_k = 0 \quad \text{if } \mathbf{G}_k < \mathbf{G}_{(c)}(d_k) \quad \text{or if } \mathbf{G}_k = \mathbf{G}_{(c)}(d_k) \text{ and } \mathrm{d}\mathbf{G}_k \leq 0 \\ \sum_{i=1}^{M} \frac{\partial \mathbf{G}_k}{\partial d_i}\mathrm{d}d_i + \frac{\partial \mathbf{G}_k}{\partial \boldsymbol{\varepsilon}}\mathrm{d}\boldsymbol{\varepsilon} = \frac{\mathrm{d}\mathbf{G}_{(c)}}{\mathrm{d}d_k}\mathrm{d}d_k \quad \text{if } \mathbf{G}_k = \mathbf{G}_{(c)}(d_k) \text{ and } \mathrm{d}\mathbf{G}_{\mathrm{k}} > 0, \end{gathered} \tag{5}$$

where $\mathbf{G}_{(c)}$ is the vector of fracture toughness in the three modes. In this type of damage evolution process, one needs to assume the distribution of the tractions in the vicinity of a single transverse crack under the three different modes of loading. For mode-I and mode-III loading, procedure for calculating the parameters β^{kl} have been discussed by Adolfsson and Gudmundson (1997, 1999). Similar to this procedure, in the present numerical simulations we assume negligible coupling between the crack surface energy due to mode-II and the others. Finally, the compliances for the cracked laminate can be expressed in terms of the change in the stiffness coefficients due to release of the residual stress. The stiffness coefficient matrix can then be obtained by inverting the compliance matrix.

In the present problem of estimating the unknown stiffness degradation, we shall restrict ourselves to first-order shear deformable laminate using the acoustic wave response. Hence, we can write the stiffness coefficients of the cracked laminate as

$$\begin{Bmatrix} N_x \\ M_x \\ V_x \end{Bmatrix} = \begin{bmatrix} \alpha_{11}C_{\mathrm{EE}_{11}} & \beta_{11}C_{\mathrm{EB}_{11}} & 0 \\ \beta_{11}C_{\mathrm{EB}_{11}} & \gamma_{11}C_{\mathrm{BB}_{11}} & 0 \\ 0 & 0 & \alpha_{55}C_{\mathrm{SS}_{22}} \end{bmatrix} \begin{Bmatrix} u^{\circ}{}_{,x} \\ \phi_{,x} \\ w_{,x} + \phi \end{Bmatrix}, \tag{6}$$

where α_{11}, β_{11}, γ_{11} and α_{55} are, respectively, the degradation factors associated with the in-plane stiffness, extension-bending coupled stiffness, bending stiffness and the transverse shear stiffness. The force vector

$$\mathbf{f} = \{ N_x \quad M_x \quad V_x \}^T$$

is assumed to have a quasi-static part (contributing in the matrix crack initiation and growth process) and a temporal part (designed to generate acoustic signal for diagnostics). We shall study the response of the degraded laminate under this temporal acoustic signal. For first-order shear deformation, x component of the displacement $u(x, z, t) = u^{\circ}(x, t) + z\phi(x, t)$ and z component of the displacement $w(x, z, t) = w(x, t)$.

Below we study the effect of variation in crack density on the degradation factors (equation (6)) using the damage evolution model discussed earlier. Graphite-epoxy laminated composite with the following properties are considered. Elastic moduli: $E_1 = 144.48\,\text{GPa}$, $E_2 = 9.632\,\text{GPa}$, $E_3 = 9.632\,\text{GPa}$; shear moduli: $G_{23} = 4.128\,\text{GPa}$, $G_{13} = 4.128\,\text{GPa}$, $G_{12} = 7.0\,\text{GPa}$; Poisson's ratio: $\nu_{12} = \nu_{13} = \nu_{23} = 0.3$ and density $\rho = 1,389\,\text{kg/m}^3$. Thickness of each ply is 2 mm. In the numerical simulations we assume straight transverse crack surfaces in cross-plies across the entire thickness. Figure 2(a)-(d) shows the set of the degradation factors for various specified crack densities at the cross-plies. In all these symmetric ply stacking sequences $\beta_{11} = 0$. It can be seen that when the cracked cross-plies consists of the major portion of the laminate thickness, the shear stiffness degradation (α_{55}) is large compared to others. Subsequently, variation in the in-plane stiffness degradation factor (α_{11}) is opposite. In all the cases, the scale of variation in the bending stiffness degradation factor (γ_{11}) is within 1.0-0.9. Figure 3(a)-(d) shows the set of the degradation factors for various specified crack densities at the cross-plies for asymmetric ply stacking configurations ($\beta_{11} \neq 0$). Owing to transverse cracks at the surfaces of the laminates (Figure 3(a)),

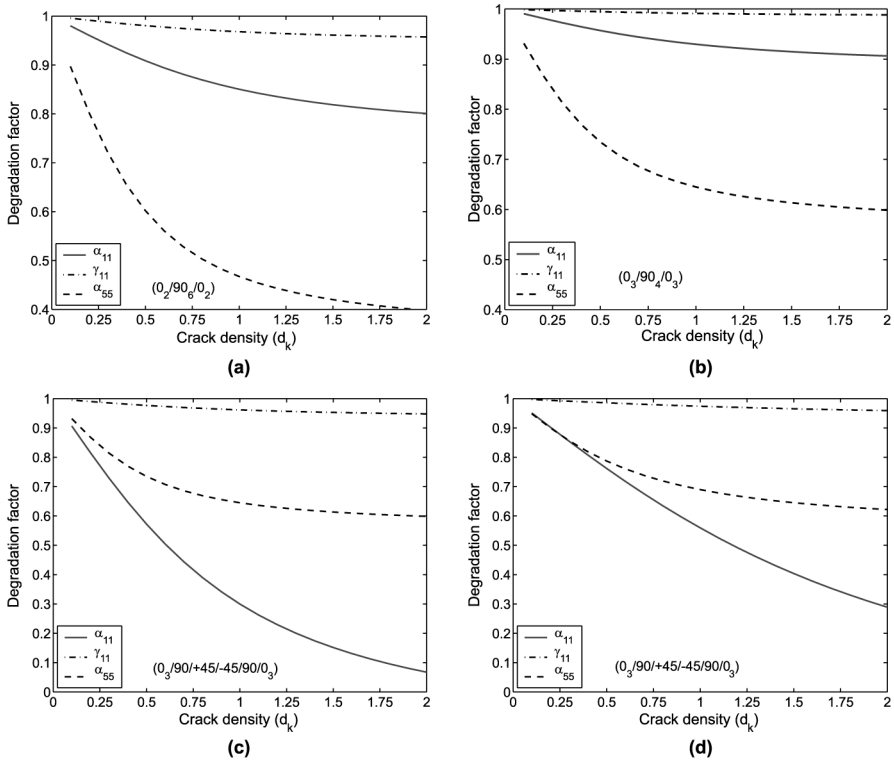

Figure 2.
Degradation factors for the ply stiffness coefficients at different transverse crack densities

Note: (a) $(0_2/90_6/0_2)$, **(b)** $(0_3/90_4/0_3)$, **(c)** $(0_3/90/+45/–45/90/0_3)$ with 100% of the specified crack density in ±45° plies and **(d)** $(0_3/90/+45/–45/90/0_3)$ with 50% of the specified crack density in ±45° plies

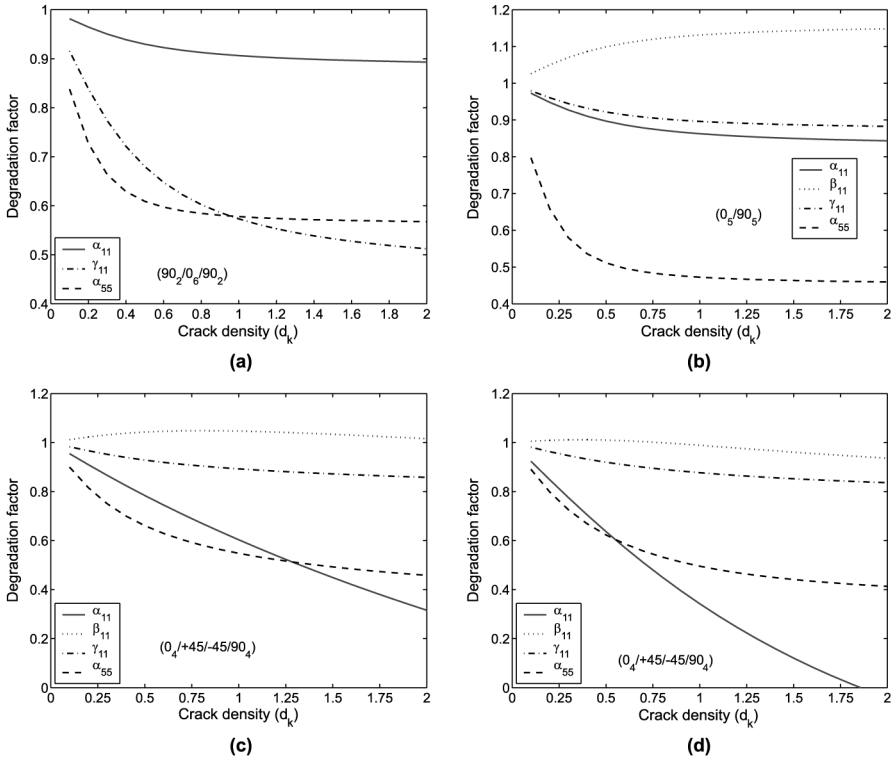

Note: (a) $(90_2/0_6/90_2)$, **(b)** $(0_5/90_5)$, **(c)** $(0_4/+45/–45/90_4)$ with 25% of the specified crack density in ±45° plies and **(d)** $(0_4/+45/–45/90_4)$ with 50% of the specified crack density in ±45° plies

Figure 3.
Degradation factors for the ply stiffness coefficients at different transverse crack densities

the degradation in the bending stiffness is large compared to the other ply stacking configurations with interior cracks. The degradation in the shear stiffness coefficient is also significant for the surface crack cases $(90_2/0_6/90_2)$ and $(0_5/90_5)$, although the variation at the higher crack densities is negligible. This is because the transverse shear profile over the laminate thickness is parabolic (apart from the discontinuities at the 0-90° interfaces causing strain jumps) and hence the major portion of the transverse shear stress is distributed over the uncracked 0° ply thickness. For asymmetric ply stacking configurations having cracked 90° plies, the scale of variation in the extension-bending coupled stiffness coefficient β_{11} is large for ply stacking configuration with maximum asymmetry $(0_5/90_5)$ as shown in Figure 3(b). Very high degradation in the in-plane stiffness coefficients as well as in the shear stiffness coefficients can be seen in Figure 3(d) for $(0_4/+45/-45/90_4)$ ply stacking which correspond to maximum matrix cracking at one surface as well as near mid-plane of the laminate.

From the above numerically simulated effects of the transverse matrix crack on the degradation factors, which show variation of these factors over a small range (1.2-0.4)

compared to the values of the stiffness coefficients themselves (similar numerical and experimental results have been reported by several authors as mentioned in the introductory discussion), it can be seen that the estimation of these factors, given the acoustic wave response of the degraded laminate, is a challenging task, but can be a useful technique for SHM. A practical approach is to develop ANN-based estimation technique, where the network can be trained off-line using numerically simulated data and can further be fine-tuned online using the measured data. Toward development of such ANN-based technique, one of the two important aspects, which has been discussed in the introduction of this paper, that is the numerically simulated acoustic wave response for off-line training of the ANN, is discussed in the next section.

3. Acoustic wave response of degraded laminate using a spectral finite element model

Spectral analysis and associated numerical techniques for studying wave interaction with material interfaces are particularly suitable for damage diagnostics. In the same line as in the interrogation strategies using acoustic device, computational simulation techniques based on spectral analysis can be efficiently integrated in SHM software. Several potentials of such strategies can be found in the works of Liu and Achenbach (1995), Aberg and Gudmundson (2000), Ishak *et al.* (2001), Xu and Liu (2002), Nag *et al.* (2002b, 2003) and Kumar *et al.* (2003). The basic framework of the SFEM employed in the present paper can be found in Doyle (1997) for isotropic solid and in Roy Mahapatra and Gopalakrishnan (2003) for laminated composite.

The basic steps in developing the SFEM for the degraded laminated composite beam type structure or laminated plate under plane strain condition are as follows. Considering a general ply stacking sequence, the governing wave equation in two-dimension (*XZ* plane shown in Figure 1) or reduced one dimension (*X* direction) is formed. In the present paper, we consider reduced on-dimensional representation by assuming first-order transverse shear deformation. After discrete Fourier transformation (DFT) of the temporal variables, the characteristic system is solved in (ω_n, k_j) pair, where ω_n is the FFT sampling frequency (controlled depending on the excitation bandwidth) and k_j is the jth mode of wave. A field interpolation technique based on the base vector from the null space of the characteristic system is then employed. The spectral element for coupled wave propagation in such beam type structure involves two nodes at the end of the element and standard finite element assembly. Frequency response over a frequency band is obtained by solving the assembled complex dynamic stiffness matrix at each sampling frequency. The temporal response can be obtained using inverse FFT under any general transient dynamic loading. For characteristic wave propagation in such beam, the high frequency limit is imposed by the unmodelled kinematics that may introduce the higher-order Lamb wave modes (first symmetric stretching mode and higher, and third anti-symmetric stretching mode and higher). Hence, the bandwidth of attached acoustic/ultrasonic device needs to be operated within the above limit. For example, one can use only the first symmetric Lamb wave mode (S_0 mode) and measure the ultrasonic response of the degraded cross-ply laminates as reported by Toyama *et al.* (2003).

In the present computational model, one single spectral element with degraded ply properties are considered first. The element formulation is such that the length

of the element can be chosen irrespective of the wavelength of excitation. Next, the element nodal degrees of freedom are condensed after the assembly of two undamaged segments on both sides of the span-wise degraded zone. The individual plies with transverse micro-cracks finally contribute in the cross-sectional stiffness when integrated over the thickness of the laminates. Finally, it becomes possible to describe the damage configuration just by prescribing three sets of parameters:

(1) degradation factors (α_{ij}, β_{ij}, γ_{ij}) describing the degraded laminate (equation (6));

(2) approximate span-wise location from where the degradation starts; and

(3) the length of the degraded zone (Figure 4(a)).

Considering similar assembly technique, the models for delamination and large transverse crack were reported by Nag *et al.* (2002b) and Kumar *et al.* (2003).

The spectral solution for primary displacement field vector is given by

$$\mathbf{u}(x,t) = \{u^{\circ}(x,t)w(x,t)\phi(x,t)\}^T = \sum_{n=1}^{N} \hat{\mathbf{u}}(x,\omega_n)e^{i\omega_n t} = \sum_{n=1}^{N}\left(\sum_{j=1}^{6} \tilde{\mathbf{u}}_{\mathbf{j}} e^{-ik_j x}\right) \mathrm{e}^{i\omega_n t}, \quad (7)$$

where $i = \sqrt{-1}$, ω_n is the frequency at nth sampling point, and k_j is the wave number associated with the jth mode of wave (forward or backward propagating or evanescent mode). u°, w and ϕ are, respectively, the reference plane longitudinal displacement, the transverse displacement and cross-sectional rotation of the first-order shear deformable beam or a plate cross-section under plane-strain condition. $\hat{\mathbf{u}} = \{\hat{u}^{\circ}\hat{w}\hat{\phi}\}^T$ represents the spectral amplitude vector corresponding to generic displacement vector $\mathbf{u}$ as functions of (x, ω_n).

$$\tilde{\mathbf{u}}_{\mathbf{j}} = \{\, \tilde{u}_j \quad \tilde{w}_j \quad \tilde{\phi}_j \,\}^T$$

represents the wave coefficient vector associated with jth mode of wave. The acoustic wave excitation, which guides the forced frequency response is written as

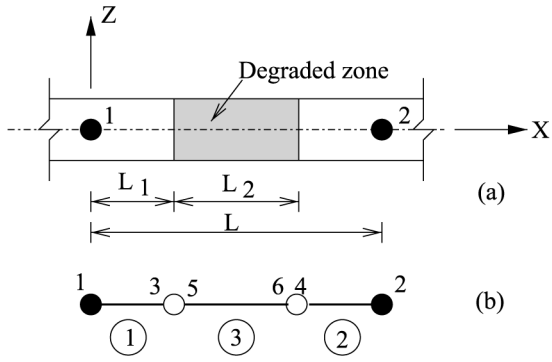

Note: (a) Composite beam segment with the degraded zone of size L_2. The whole segment is represented by the end nodes 1 and 2 of the spectral element. **(b)** The element local configuration showing the internal element numbers (1), (2) and (3) by circles and the associated nodes 1-3, 2-4, and 5-6

Figure 4.

$$\mathbf{f}(x,t) = \sum_{n=1}^{N} \hat{\mathbf{f}}(x,\omega_n) e^{i\omega_n t}, \tag{8}$$

where the spatial variation of the force amplitude $\hat{\mathbf{f}}(x, \omega_n)$ can be lumped consistently using the spectral displacement shape function (Roy Mahapatra and Gopalakrishnan, 2003) on the element nodes. Next we compute k_j by solving the dispersion relation and reduce the number of unknown wave coefficients using the base vectors from the null space of the characteristic system. This gives us a matrix called amplitude ratio matrix whose rows are the base vectors and each column is associated with a particular mode of wave $\tilde{u}e^{-ik_j x}$. The force boundary conditions are then used to eliminate the unknown wave coefficient vector $\tilde{\mathbf{u}}$ and the dynamic stiffness matrix is formed. The detail derivation can be found in Roy Mahapatra and Gopalakrishnan (2003) and Nag *et al.* (2003) and we shall skip those detail here and only show the steps by which the degraded zone is embedded within the one-dimensional element without imposing any limitation on its length in terms of the wavelength.

3.1 Spectral element with embedded degraded zone

The location of the two nodes of the spectral elements with embedded degraded zone in a beam is shown in Figure 4(a), where the plies are stacked along the thickness (z direction). In absence of degradation, one spectral element between nodes 1 and 2 is sufficient for analysis. The degradation of the ply property is modelled using the constitutive equation (6). Four more nodes are introduced to model the degraded zone (element (3)) as shown in Figure 4(a). In practical situation, it may so happen that the matrix crack density in laminates may decrease with some gradation from the central portion of the damaged zone. In such case, the elements (1) and (3) can be used with such functionally graded laminate properties based on the same constitutive model as discussed in equation (6).

The kinematic assumption of continuity of displacements and rotations at the internal element nodes 3, 5 and 4, 6 leads to

$$\hat{\mathbf{u}}_5 = \left\{\hat{u}_5^0 \hat{\omega}_5 \hat{\phi}_5\right\}^T = \hat{\mathbf{u}}_3, \quad \hat{\mathbf{u}}_6 = \left\{\hat{u}_6^0 \hat{\omega}_6 \hat{\phi}_6\right\}^T = \hat{\mathbf{u}}_4. \tag{9}$$

From equilibrium of the nodal forces and moments at the left interface (between nodes 3 and 5) and at the right interfaces (between nodes 4 and 6), we get, respectively,

$$\hat{\mathbf{f}}_3 + \hat{\mathbf{f}}_5 = 0, \quad \hat{\mathbf{f}}_4 + \hat{\mathbf{f}}_6 = 0. \tag{10}$$

The element equilibrium equation at a particular sampling frequency ω_n for the lth internal element ($l = 1, 2, 3$) with nodes p and q can be written as

$$\begin{bmatrix} \hat{\mathbf{K}}_{11}^{(l)} & \hat{\mathbf{K}}_{12}^{(l)} \\ \hat{\mathbf{K}}_{21}^{(l)} & \hat{\mathbf{K}}_{22}^{(l)} \end{bmatrix}_{(6\times6)} \begin{Bmatrix} \hat{\mathbf{u}}_p \\ \hat{\mathbf{u}}_q \end{Bmatrix} = \begin{Bmatrix} \hat{\mathbf{f}}_p \\ \hat{\mathbf{f}}_q \end{Bmatrix}, \tag{11}$$

where $\hat{\mathbf{K}}_{(6\times6)}^{(l)}$ is the complex dynamic stiffness matrix (Roy Mahapatra and Gopalakrishnan, 2003) as function of the sampling frequency ω_n, wave number k_j, $j = 1, \ldots, 6$, stiffness coefficients and the length. By assembling equation (11) for the three internal elements (1), (2) and (3), we get

$$\begin{bmatrix} \hat{\mathbf{K}}_{11}^{(1)} & \hat{\mathbf{K}}_{12}^{(1)} & 0 & 0 \\ \hat{\mathbf{K}}_{21}^{(1)} & \hat{\mathbf{K}}_{22}^{(1)} + \hat{\mathbf{K}}_{11}^{(2)} & \hat{\mathbf{K}}_{12}^{(2)} & 0 \\ 0 & \hat{\mathbf{K}}_{21}^{(2)} & \hat{\mathbf{K}}_{22}^{(2)} + \hat{\mathbf{K}}_{11}^{(3)} & \hat{\mathbf{K}}_{12}^{(3)} \\ 0 & 0 & \hat{\mathbf{K}}_{21}^{(3)} & \hat{\mathbf{K}}_{22}^{(3)} \end{bmatrix}_{(12\times12)} \begin{Bmatrix} \hat{\mathbf{u}}_1 \\ \hat{\mathbf{u}}_3 \\ \hat{\mathbf{u}}_4 \\ \hat{\mathbf{u}}_2 \end{Bmatrix} = \begin{Bmatrix} \hat{\mathbf{f}}_1 \\ 0 \\ 0 \\ \hat{\mathbf{f}}_2 \end{Bmatrix}. \tag{12}$$

On condensation of the degrees of freedom at the internal nodes 3 and 4 and assuming that no force is applied on the degraded zone, equation (12) becomes

$$\hat{\mathbf{K}}_{(6\times6)} \begin{Bmatrix} \hat{\mathbf{u}}_1 \\ \hat{\mathbf{u}}_2 \end{Bmatrix} = \begin{Bmatrix} \hat{\mathbf{f}}_1 \\ \hat{\mathbf{f}}_2 \end{Bmatrix}, \tag{13}$$

where the submatrices of the new dynamic stiffness matrix $\hat{\mathbf{K}}$ are defined as

$$\hat{\mathbf{K}}_{11} = \hat{\mathbf{K}}_{11}^{(1)} - \hat{\mathbf{K}}_{12}^{(1)} \left(\hat{\mathbf{K}}_{22}^{(1)} + \hat{\mathbf{K}}_{11}^{(2)} \right)^{-1} \mathbf{X}_2, \tag{14}$$

$$\hat{\mathbf{K}}_{12} = \hat{\mathbf{K}}_{12}^{(1)} \left(\hat{\mathbf{K}}_{22}^{(1)} + \hat{\mathbf{K}}_{11}^{(2)} \right)^{-1} \hat{\mathbf{K}}_{12}^{(2)} \mathbf{X}_1^{-1} \hat{\mathbf{K}}_{12}^{(3)}, \tag{15}$$

$$\hat{\mathbf{K}}_{21} = \hat{\mathbf{K}}_{21}^{(3)} \mathbf{X}_1^{-1} \hat{\mathbf{K}}_{21}^{(2)} \left(\hat{\mathbf{K}}_{22}^{(1)} + \hat{\mathbf{K}}_{11}^{(2)} \right)^{-1} \hat{\mathbf{K}}_{21}^{(1)}, \tag{16}$$

$$\hat{\mathbf{K}}_{22} = \hat{\mathbf{K}}_{22}^{(3)} - \hat{\mathbf{K}}_{21}^{(3)} \mathbf{X}_1^{-1} \hat{\mathbf{K}}_{12}^{(3)}, \tag{17}$$

$$\mathbf{X}_1 = \left(\hat{\mathbf{K}}_{22}^{(2)} + \hat{\mathbf{K}}_{11}^{(3)} \right) - \hat{\mathbf{K}}_{21}^{(2)} \left(\hat{\mathbf{K}}_{22}^{(1)} + \hat{\mathbf{K}}_{11}^{(2)} \right)^{-1} \hat{\mathbf{K}}_{12}^{(2)}, \tag{18}$$

$$\mathbf{X}_2 = \hat{\mathbf{K}}_{21}^{(1)} + \hat{\mathbf{K}}_{12}^{(2)} \mathbf{X}_1^{-1} \mathbf{K}_{21}^{(2)} \left(\hat{\mathbf{K}}_{22}^{(1)} + \hat{\mathbf{K}}_{11}^{(2)} \right)^{-1} \hat{\mathbf{K}}_{21}^{(1)}. \tag{19}$$

Equation (13) is the equilibrium equation for the spectral element with embedded degraded zone, where only the degrees of freedom at the end nodes 1, 2 need to be used while forming the global system of a damaged structural component. The global system is solved at each sampling frequency ω_n, $n = 1, \ldots, N$, where N is the Nyquist frequency. Time history of any quantity such as displacement, strain or their rate can be simulated by using inverse FFT.

4. Effect of crack density on the acoustic wave response

Two types of transient loading, one is a Gaussian force history with duration of 30 μs and the other is a tone-burst signal modulated at 75 kHz and a duration of 80 μs is considered in the present analysis. The time histories and the corresponding frequency spectrum are, respectively, shown in Figure 5(a) and (b). A 0.8 m long cantilever beam with

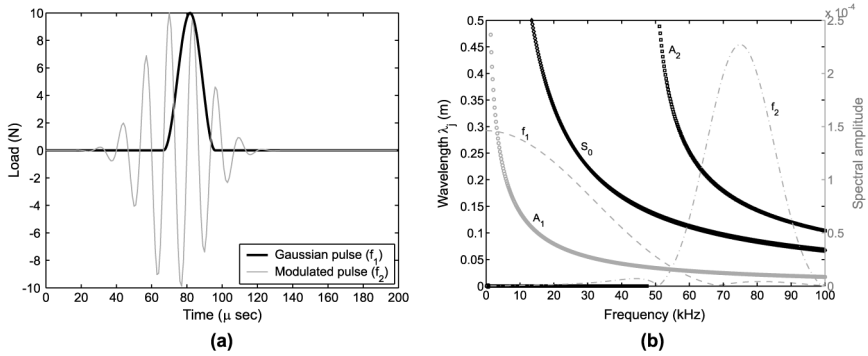

Note: (a) A broadband gaussian pulse and a single frequency tone-burst pulse for diagnostic wave generation. **(b)** Frequency spectrum of these pulses showing the wavelengths of interrogation in a $(0_2/90_6/0_2)$ graphite-epoxy beam

Figure 5.

graphite-epoxy laminate material properties given in Section 2 and $(0_2/90_6/0_2)$ ply stacking is considered. The wavelengths ($\lambda_j = 2\pi/k_j$) of propagation at various frequencies are shown by thick dotted lines in Figure 5(b). The S_0 mode is the bulk longitudinal wave mode or the first symmetric Lamb wave mode. The A_1 mode is the flexural wave mode or the first anti-symmetric Lamb wave mode. The A_2 mode is the transverse wave mode or the second anti-symmetric Lamb wave mode. It is important to note the numerical values of the wavelengths while using the broad-band Gaussian excitation (f_1) or the narrow-band tone-burst excitation (f_2). For sensitive interrogation of a probable size of the degraded zone, one needs to have the desired excited wavelengths, the smallest of which must be less than twice the size of the degraded zone. Hence from Figure 5(b) it can be observed that the narrow-band excitation (f_2) shown in the figure can be used optimally to obtain sensitive response from a degraded zone of size ≈ 2.5 cm by A_1 mode. On the other hand, a higher size of degraded zone can be interrogated in the same A_1 mode using the broad-band excitation (f_1). Similarly, a higher size of degraded zone can also be interrogated in S_0 or A_2 mode sensitively while using the narrow-band excitation.

In Figure 6(a) we show the simulated time history of the tip velocity when the broad-band load (f_1) is applied in transverse direction at the tip of the 0.8 m graphite-epoxy cantilever beam having a 5 cm degraded zone at the mid-span. The degraded zone consists of transverse matrix crack at the cross-plies with uniform crack density of $d_k = 2$. The additional peaks near 0.5 ms indicate the scattering from the degraded zone in A_1 mode with the highest possible group speed $c_g = d\omega_n/dk_j$ of the excited wave packet at ≈ 40 kHz (Figure 5). To quantify the change in the corresponding frequency response, we compute the difference between the spectral amplitude of the transverse displacement for degraded and undegraded beam. The absolute value of this difference, which, in other words is the change in the forced resonance under the broad-band excitation, is denoted by $\Delta u_r(f_1)$. The same, under the narrow-band excitation is denoted by $\Delta u_r(f_2)$. Both these quantities over the respective frequency bands and wavelength range are shown in Figure 6(b). This figure shows the possibility of further fine-tuning of the wavelength-selective excitation corresponding to the frequencies at which maximum sensitivity can be achieved. However, one should note that such sensitivity is associated

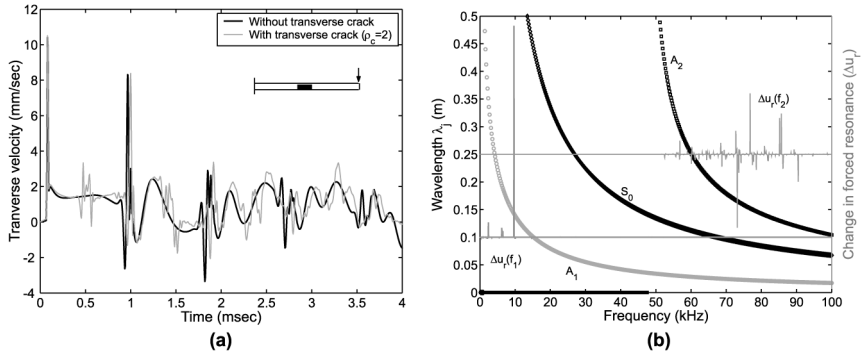

Note: (a) Transverse velocity at the tip of the $(0_2/90_6/0_2)$ graphite-epoxy cantilever beam with a mid-span 5cm zone with uniform transverse crack density of $d_k = 2$. **(b)** Change in the forced resonance (Δu_r) due to the cracked zone under excitation using loads f_1 and f_2 (Fig. 5) over wavelength and frequency bands

Figure 6.

with the structural boundary, the size of the degraded zone and the degradation factors. Also, for practical development in highly tunable frequency-selective acoustic wave interrogation technique, one needs to include additional effects, such as deviation due to the modelling assumptions, several uncertainties, etc.

To simulate the effect of graded crack density, we consider a 7.5 cm zone at both sides of the 5 cm uniformly cracked zone ($d_k = 2$), in which the crack density is assumed to vary from 2 to 0 linearly. Instead of a single spectral element as in the previous example, three spectral elements with step-wise graded crack densities are used over each of the 7.5 cm zone. One spectral element with $d_k = 2$ is used over the mid-span 5 cm zone. Two spectral elements with original stiffness properties are used for the fixed-end segment and the free-end segment. The complete model consists of nine spectral elements. It can be seen from Figure 7(a) and (b) that the scattered wave for the graded case arrives before the ungraded case having smaller zone (5 cm). Under the narrow-band excitation,

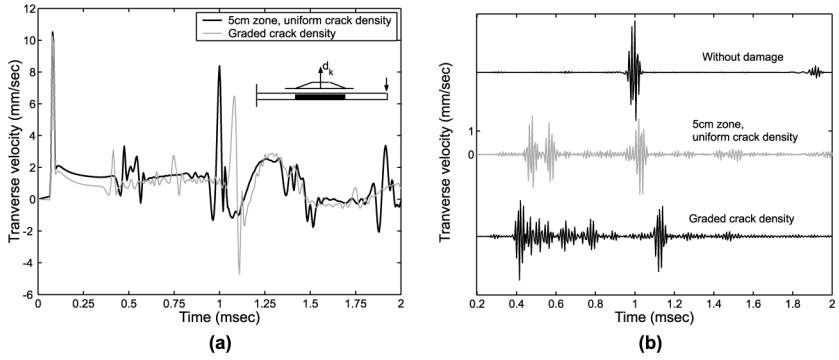

Note: (a) Response under broad-band excitation (f_1). **(b)** Response under narrow-band excitation (f_2)

Figure 7.
Transverse velocity at the tip of the $(0_2/90_2/0_2)$ graphite-epoxy cantilever beam with a mid-span 5 cm zone having uniform transverse crack density of $d_k = 2$ and graded crack density over 7.5 cm zones at both sides of the 5 cm zone

two distinct peaks can be seen at 0.45 and 0.6 ms for the ungraded case, where as smaller peaks can be seen for the graded case, which are due to step-wise gradation of the crack density. This resembles more realistic response, and while using smaller wavelengths one may expect many small peaks due to scattering of the higher-order Lamb wave modes at the individual crack surfaces, which are not included in the present model.

The above simulations show the usefulness of the spectral element model for generation of acoustic wave response which can be used for training the ANN. Also, the computational efficiency of the spectral element model is found to be very high compared to other finite element models. We consider Fourier spectral data as the input to the ANN. Therefore, for repeated spectral element analysis with varying crack density, location and size of the degraded zone, one can take advantage of computing the spectral amplitude of displacements, strains or their rate. However, the second of the two important aspect as discussed in the introduction, that is the large size of the spectral data (when taken with fine sampling) and keeping in view the possibility of frequency band selectivity, the concept of ANN with dimensionally reduced data are discussed in the next section.

5. Dimensionality reduction of spectral data by independent component analysis (ICA)

A common problem encountered in disciplines such as data analysis, signal processing, and neural network research, is finding a suitable transformed representation of multivariate data. For conceptual and computational simplicity, such a representation is often sought as a linear transformation of the original data. It is important for the subsequent analysis of the data, weather it be pattern recognition, data compression, visualization, etc. that the data are represented in a manner that facilitates the analysis. Several well-known linear transformation methods, e.g. factor analysis (Harman, 1967), principal component analysis (PCA) (Oja, 1982) and projection pursuit (Friedman, 1987) can be used for the above purpose. These methods define a principle that tell which transformation is optimal. The definition of optimality depends on the method used. The optimality may be defined in the sense of optimal reduction of dimensions, statistical interestingness of the resulting data, simplicity of the transformation, or depending on the specific applications, we can have mixed criteria. The above methods for finding linear transformations are second-order methods. This means that the methods find the representation using only the information contained in the covariance matrix of the data. If the data has normal or Gaussian distribution, then the second order methods can determine the complete information inside the data. In general, the second order methods fail to determine the meaningful (meaningful is task dependent property) representation of the data. Also, the second order methods fail to extract the features from the data if the data are redundant. But the higher-order methods seem to be able to find meaningful representations in a wide variety of applications (Friedman, 1987).

Recently, a particular method for finding a transformation of data, called ICA, has gained wide-spread attention. The main objective of this method is to find a transformation in which the components of transformed data are statistically as independent from each other as possible. ICA can be applied for blind source separation, feature extraction and exploratory data analysis. The promising application of ICA is feature extraction. The extracted feature vectors from the ICA analysis are as independent from each other as possible, i.e. the extracted features will not provide any

information that could be used to predict the other features. ICA method has been successfully implemented in many practical problems of feature extraction (Olshausen and Field, 1996, 1997). Application of feature extraction using ICA on data compression and pattern recognition are important research topics.

5.1 ICA algorithm

The input data for the ICA is a N-dimensional random vector, and it is denoted as $\mathbf{x} = \{x_1, x_2, \ldots, x_N\}^T$. In our present problem, $\mathbf{x} = \hat{\mathbf{u}}$, where $\hat{\mathbf{u}}$ is the Fourier spectrum of displacement and N is the Nyquist frequency in FFT. The main objective of the ICA is that of finding the transformation $\mathbf{y} = \{y_1, y_2, \ldots, y_M\}^T$, so that the components y_m, $m = 1, \ldots, M$; $M < N$ are as independent as possible, in the sense of maximizing some objective function $F(s)$ that measures independence. The statistical properties of the ICA method depend on the objective function used. The detail of the selection of different of objective functions and their advantage have been discussed by Hyvarinen (1990). The transformation from $\mathbf{x}$ to $\mathbf{s}$ can be mathematically expressed as

$$\mathbf{s} = G(\mathbf{x}). \tag{20}$$

Based on the nature of the transformation function G, we can have linear or non-linear ICA algorithm. The following are the basic assumptions in the ICA model:

- all the independent components (ICs) $\mathbf{s}_i$, with possible exception of one component, must be non-Gaussian;
- the number of observed linear mixtures N (dimension of the input data) must be at least as large as the number of ICs M, i.e. $N \geq M$;
- in case of linear ICA, the transformation matrix must be of full column rank; and
- $R \gg N$, where R is the number of patterns.

After choosing the objective function and the method of transformation (linear or non-linear), one needs to decide how to optimise the transformation. It has been shown by Hyvarinen (1990) that the layer of neurons whose weights are modified using simple Hebbian learning algorithm with weight decay, not only stops the weights growing without bound, but also causes the weights to converge to optimal value. In other words, the weight decay has the amazing effect of not only causing the weight increase for stabilization, but also causing the convergence of the weights to the values that are optimal to extract the maximum information from the input data. One advantage of this learning algorithm is that it is completely homogeneous, i.e. the operations carried out at each neurons are identical. This is essential if one needs to take the full advantage of parallel processing (Hyvarinen, 1990).

The architecture of the ICA network is shown in Figure 8. It has N input neurons and M output neurons. Let the inputs to the network be denoted by the N dimensional vector $\mathbf{x}$, the output by the M dimensional vector $\mathbf{y}$ and the weight connections between the input and output neurons by the matrix $\mathbf{w}$. Assume that we are going to extract the M ICs from the N dimensional input vector, $M < N$ and the input vector is a random variable. The dynamics of the neural network can be expressed mathematically using the following equations.

Let s_m and y_m be the activation value and the output of the mth output neuron, respectively.

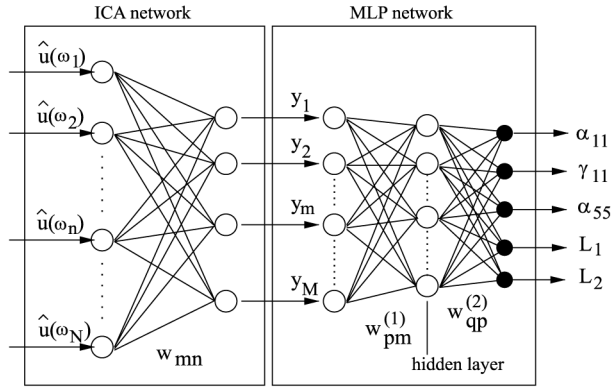

Figure 8.
Schematic diagram showing the ICA network connected to the MLP network

$$s_m = \sum_{j=1}^{N} w_{mj} x_j, \quad y_m = f(s_m), \quad m = 1, \ldots, M \tag{21}$$

where $f(s_m)$ is the activation function. After calculating the activation values of the output neurons, the activation values are passed through the same weights to the input neurons as inhibition to calculate the sphered activation value of the input neurons. The sphered activation value ($\bar{x}_n$) of the nth input neuron is given by

$$\bar{x}_n = x_n - \sum_{m=1}^{M} w_{mn} s_n, \quad n = 1, \ldots, N. \tag{22}$$

The weights of the ICA network are updated using simple Hebbian learning rule. The change in the weights are calculated after each pattern ($r = 1, \ldots, R$) is presented to the network and is given by

$$\Delta w_{mn} = \eta y_m \bar{x}_n, \tag{23}$$

where η is the learning rate parameter. As we can observe from the above equation that the weights will grow without any bound. This problem is avoided using the orthonormalization of the weight vectors

$$w_{mn} = \frac{w_{mn}}{\sqrt{\mathbf{w}_m^T \mathbf{w}_m}}. \tag{24}$$

Each row of weight matrix $\mathbf{w}$ form the basis vector for the ICs. In order to avoid the different weight vectors from converging to same value, we must decorrelate the outputs $\mathbf{w}_1^T x, \ldots, \mathbf{w}_M^T x$ after every iteration. A simple way of achieving decorrelation is a deflation scheme based on a Gram-Schmidt like decorrelation (Oja and Hyvarinen, 2004). This means that we estimate the weight vectors one by one. When we estimate M vectors ($\mathbf{w}_1, \ldots, \mathbf{w}_p, \mathbf{w}_{p+1}, \ldots, \mathbf{w}_M$), each of them representing a row of the weight matrix $\mathbf{w}$, we run the above algorithm by computing $\mathbf{w}_{p+1}$ from its previous projections as

$$\mathbf{w}_{p+1} = \mathbf{w}_{p+1} - \sum_{j=1}^{p} \mathbf{w}_{p+1} \mathbf{w}_j^T \mathbf{w}_j. \tag{25}$$

6. MLP network with independent components as input

The output of the ICA network is fed as input to a MLP network having one hidden layer. The output of the MLP network, in the present problem, are the stiffness degradation factors α_{11}, γ_{11}, α_{55}, the location of the degraded zone, which is defined by the span-wise coordinate L_1 of one approximate end of the zone with matrix cracks, and the span of the degraded zone itself which is defined by L_2. In the previous work of Garg *et al.* (2004), a simpler network architecture with α_{11}, L_1 and L_2 as the output was used. The main difference in the present strategy is that the ICs having reduced dimension compared to the original spectral data are used as input instead of the original spectral data. Also the number of MLP network output is increased from three to five. The architecture of this reduction-prediction network is shown in Figure 8.

6.1 Network training and testing

To demonstrate the numerical efficiency of the proposed strategy for estimating the degraded properties, location and size in a laminated composite beam, we perform the following case study. We consider a 0.8 m long $[0_2/90_6/0_2]$ graphite-epoxy cantilever beam as described earlier. We perform the network training as well as the testing using the SFEM-based data. The data set consists of the following:

$$\begin{aligned} L_1 &\in [0.2\,\text{m}, 0.7\,\text{m}] \text{ in steps of } 0.02\,\text{m} \\ L_2 &\in [0.01\,\text{m}, 0.02\,\text{m}] \text{ in steps of } 0.01\,\text{m} \\ \alpha_{11} &\in [0.800829, 0.980026] \\ \gamma_{11} &\in [0.957301, 0.995747] \\ \alpha_{55} &\in [0.397998, 0.897106]\,, \end{aligned}$$

which gives a total of 10,000 samples (patterns). The ply stacking sequence is symmetric and the transverse matrix cracks are assumed only in the 90° ply throughout the thickness. The sets of (α_{11}, γ_{11}, α_{55}) are generated using the model of Adolfsson and Gudmundson (1997) and its numerical implementation aspect is discussed in Section 2. Note that the range space of the degradation factors is very narrow, which makes the estimation a difficult task, even if we perform appropriate normalization in an expanded scale. The broad-band excitation shown in Figure 5(a) and (b) is applied at the tip of the cantilever beam in transverse direction. Transverse displacement spectrum $\hat{w}(\omega_n), n = 1, \ldots, N$; $N = 2,048$ for each of the parametric sets (features) is obtained by spectral finite element analysis. This complex-valued spectrum is then converted into the amplitude spectrum and the phase spectrum. Further, the amplitude spectrum is converted into $\log_{10}$ scale, since the Fourier spectral amplitude (or intensity, as conventionally dealt in vibrational spectroscopy) is sensitive in the logarithmic scale. Removing the spectral component at $\omega_1 = 0$ from the simulated spectra, which is just a numerical artefact of the symmetry property of the frequency axis in FFT, we have individual sample of size $2 \times 2,047$. Out of 10,000 sample generated, 9,000 samples randomly chosen are used for training and rest of the 1,000 samples are used for testing the network. The total size of the input data for ICA is $2 \times 2,047 \times 10,000$, which means the testing data also be fed through the ICA network. For newly acquired spectral data to be used for testing or actual identification using the already trained reduction-prediction network, one first need to transform this input data

through the ICA network (Figure 8), i.e. by using the weight matrix $\mathbf{w}$ to arrive at the ICs. The ICs are then fed as input to the MLP network.

6.1.1 Computation of independent components (ICs). The weight matrix $\mathbf{w}$ is constructed using $2,047 \times 10,000$ data for amplitude and $2,047 \times 10,000$ data for phase, separately. We employ the FastICA (fixed-point) algorithm (Hyvarinen, 1990). Before this is done, we need to study the nature of correlated data that we have as the input. Since, the output of the ICA gives us the almost uncorrelated data, i.e. $E(\mathbf{y}\mathbf{y}^T) = \mathbf{I}$, it is essential to check whether the original data can be dimensionally reduced, i.e. what if the weight matrix $\mathbf{w} = \mathbf{C}^{-1/2}$, where $\mathbf{C} = E(\mathbf{x}\mathbf{x}^T)$ is the correlation matrix, such that $E(\mathbf{x}\mathbf{x}^T) = \mathbf{I}$. Therefore, the accuracy of the dimensionally reduced data will depend on how much characteristic information is preserved in terms of the eigenvalues of the correlation matrix. This is the basic principal behind the PCA (Haykins, 2001), where the eigen space is truncated by considering the dominant eigenvalues. However, in PCA, this truncated eigen space does not ensure that the maximum amount of information is preserved, and therefore we perform the ICA to extract the uncorrelated ICs rather than just the principal components.

Figure 9(a) and (b), respectively, shows the distribution of the magnitude of the eigenvalues of the correlation matrices constructed from spectral amplitude and phase data. We consider the first 500 eigen pairs in the decreasing order of the eigenvalues for constructing the weight matrix $\mathbf{w}_{(500\times2,047)}$ from ICA. It can be seen from Figure 9(a) and (b) that the eigenvalues are significantly small after the first 100 components. Through ICA, we compute the ICs corresponding to the spectral amplitude and the phase, each of them having size $500 \times 10,000$. For spectral amplitude, we have the largest remaining eigenvalue 39.0792, the smallest remaining eigenvalue 0.0292, sum of the removed eigenvalues 7.3216 and 98.24 per cent of the non-zero eigenvalues retained. For phase, we have the largest remaining eigenvalue 54.6456, the smallest remaining eigenvalue 0.4578, sum of the removed eigenvalues 255.615 and 80.51 per cent of the non-zero eigenvalues retained.

6.1.2 Training and testing of the MLP network. The total number of the neurons in the input layer of the MLP network is $M = 1,000$ (500 for spectral amplitude and 500 for phase). The number of output neurons is five. Pattern-wise training approach has been adopted in this study. Patterns (sample from 9,000 spectral data set) are presented randomly without any normalization. This particular strategy is keeping in the view of making such ICA-MLP network capable of using online data acquired after the network has already been trained with some extent of reliability. The output data are normalized in the scale $[-5, 5]$.

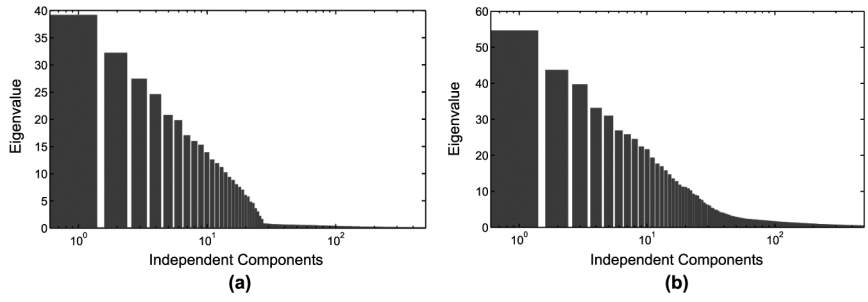

Figure 9.
Eigen space of the correlation matrix of the input data; (a) spectral amplitude; and (b) phase

The number of neurons in the single hidden layer is taken as 800. Such a number of hidden neurons is chosen based on the following steps as discussed by Suresh *et al.* (2003).

(1) Select the network with minimal configuration.

(2) Train the network until the total error (TE) < 0.002.

(3) Calculate the generalization error (GE).

(4) If GE > 0.002 then increase the number of hidden node, go to step 2, else stop.

This process is repeated until TE and GE is less than the certain prescribed value.

Bipolar sigmoidal activation function is used at the hidden layer and linear activation function is used in the output layer. Error back propagation algorithm is used with a small learning rate of 0.003. Decrease in the mean square error (MSE) over the number of training epoch is shown in Figure 10. Apart from the root mean square (RMS) error, which is commonly used in supervised learning, we also compute a more complete measure of accuracy called $\mathscr{R}_2$ estimate given by

$$\mathscr{R}_2 = 1 - \frac{\mathrm{SST}}{\mathrm{SSR}}, \tag{26}$$

where

$$\mathrm{SSR} = \frac{1}{Q}\sum_{q=1}^{Q}(y_q - \bar{y})^2, \quad \mathrm{SST} = \frac{1}{Q}\sum_{q=1}^{Q}(y_q - \hat{y}_q)^2, \tag{27}$$

Q is the total number of samples (training or testing), y_q are the actual output, $\bar{y}$ is their mean and $\hat{y}_q$ are the output predicted by the network. Table I shows the performance of the network. The $\mathscr{R}_2$ estimate shows very good accuracy, since all the output are predicted with $\mathscr{R}_2 \approx 1$. Figures 11-15 show the comparisons of the output parameters during testing with the actual values. The results show satisfactory accuracy of the individual prediction. Although there are few scatters

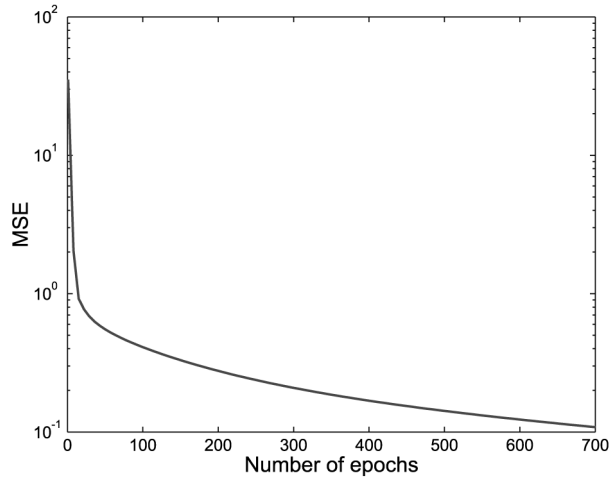

Figure 10.
Mean square error (MSE) vs the number of training epochs

in the predictions in Figures 11-15, such level of scatters can be expected in experimental prediction as well.

7. Conclusions

A micro-mechanics model of stiffness degradation due to transverse matrix cracking in composite laminates is incorporated in a SFEM to study the effect of matrix crack density on the acoustic wave response. Several aspects related to acoustic wave interrogation technique and frequency band sensitivity of damaged laminated composite beam type structures are discussed in detail. The choice on the type of excitation signal depending on the size of the degraded zone are illustrated by numerical simulation. Computationally fast and accurate analysis over broad frequency band is of particular advantage while using the proposed

Table I.
Network performance after 725 training epochs

	α_{11}	γ_{11}	α_{55}	L_1	L_2
RMS (training)	0.0066	0.0014	0.0170	0.0425	0.0086
RMS (testing)	0.0116	0.0025	0.0294	0.0644	0.0142
$\mathscr{R}_2$ (training)	0.9852	0.9851	0.9852	0.9200	0.9773
$\mathscr{R}_2$ (testing)	0.9539	0.9537	0.9572	0.8087	0.9354

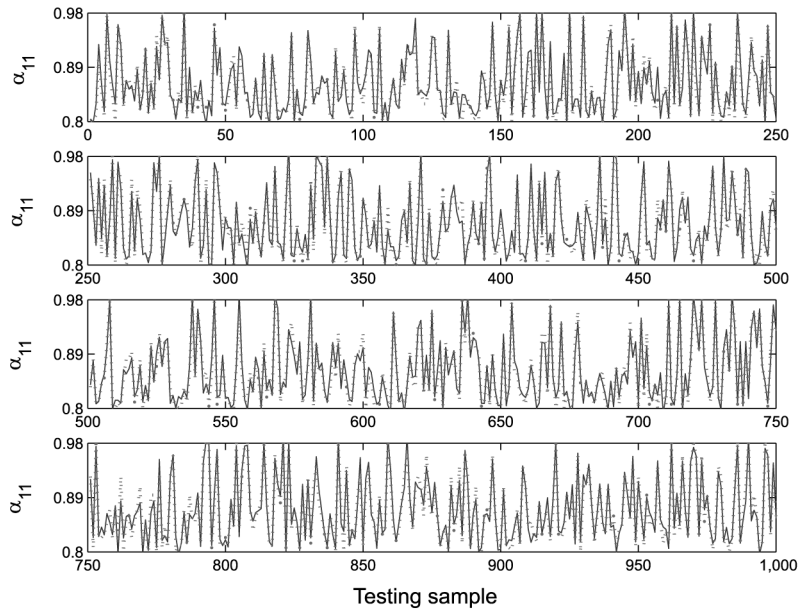

Figure 11.
Comparison of α_{11} predicted by the network during testing with the actual values

Note: Actual values are shown by dotted line and the predicted values are shown by solid line

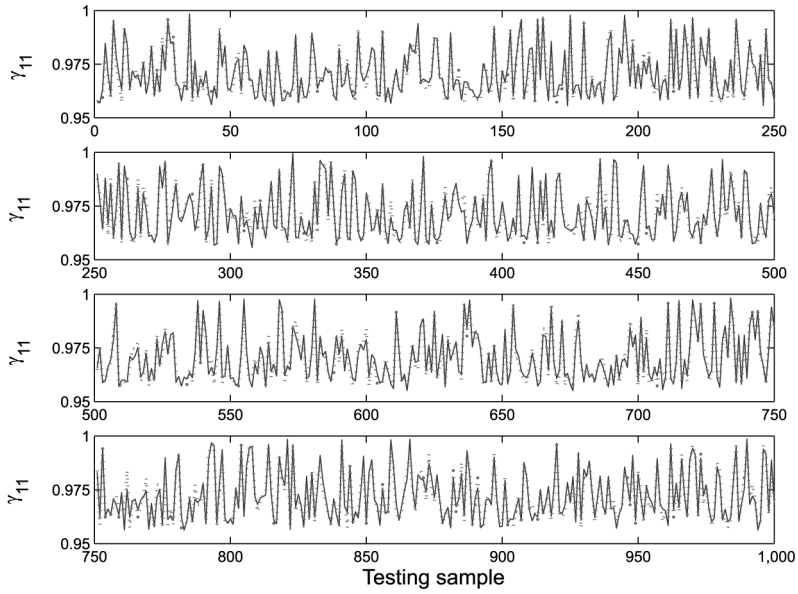

Figure 12.
Comparison of γ_{11} predicted by the network during testing with the actual values

Note: Actual values are shown by dotted line and the predicted values are shown by solid line

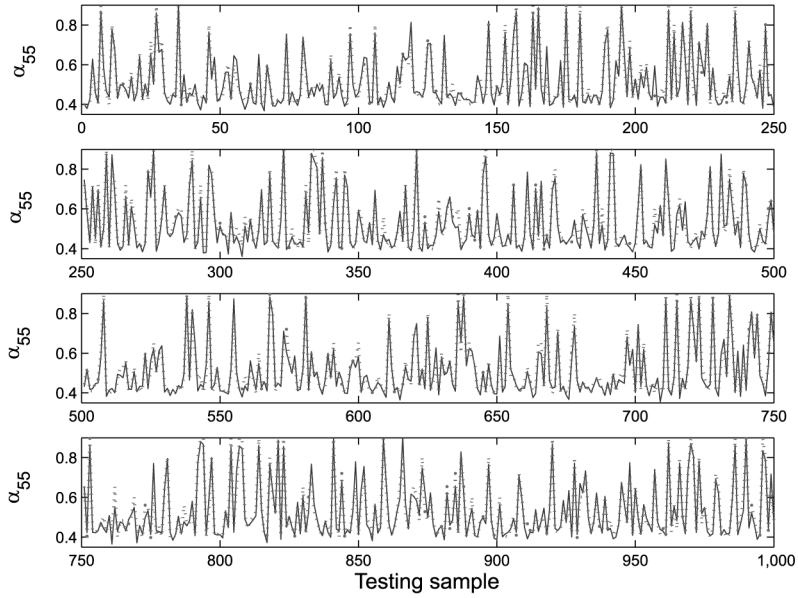

Figure 13.
Comparison of α_{55} predicted by the network during testing with the actual values

Note: Actual values are shown by dotted line and the predicted values are shown by solid line

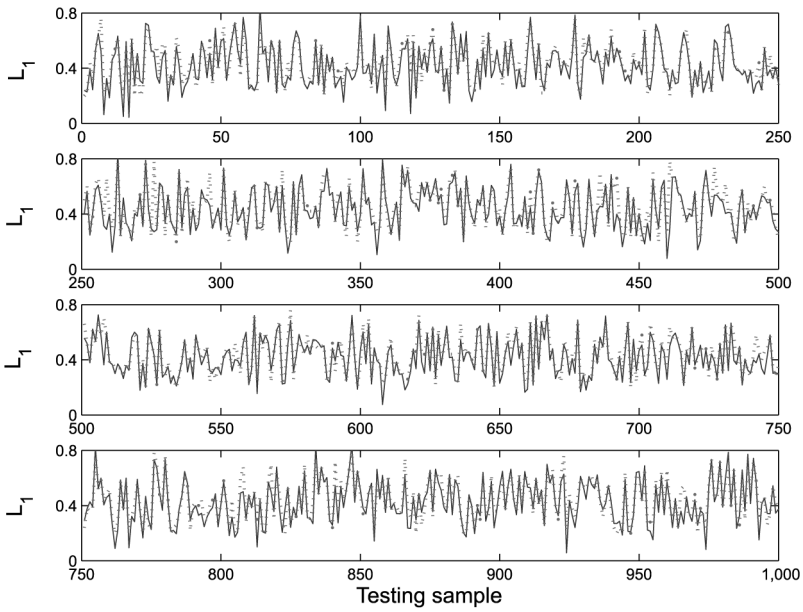

Note: Actual values are shown by dotted line and the predicted values are shown by solid line

Figure 14.
Comparison of L_1 predicted by the network during testing with the actual values

SFEM having embedded degraded zone. Development of practical approach in SHM using such acoustic wave interrogation technique appears promising, provided appropriate softcomputing tools, such as ANN, can be employed.

Two main aspects toward development of the reduction-prediction network are focused in this paper. First is the efficient numerical simulation for generation of model-based data, which can be used for off-line training and testing of the network. Second is the handling of large size of the high-resolution data and frequency band selectivity for future online measurements. Broad-band spectral data are used in the present approach to first develop the reduction network. This network transforms the spectral data into a lower dimensional non-redundant spectral data. These data are fed to the MLP network to estimate the stiffness degradation factors, location and size of the degraded zone. Performance of this reduction-prediction network using numerically simulated data shows high accuracy while estimating all the five parameters. There are several future applications of the proposed approach related to SHM. Among the major challenging issues are the appropriate modelling technique for complex damage process and quantification of the damage state in composite, cost-effective and reliable acoustic wave response simulated by these models, and finally the development of real-time self-learning ANN with tunable frequency band.

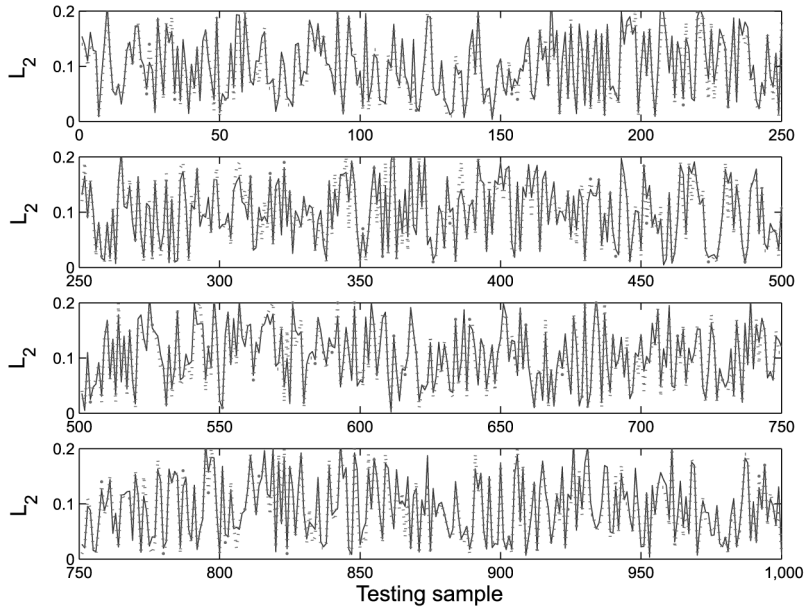

Note: Actual values are shown by dotted line and the predicted values are shown by solid line

Figure 15.
Comparison of L_2 predicted by the network during testing with the actual values

References

Aberg, M. and Gudmundson, P. (2000), "Micromechanical modeling of transient waves from matrix cracking and fiber fracture in laminated beams", *International Journal of Solids and Structures*, Vol. 37, pp. 4083-102.

Abrate, S. (1991), "Matrix cracking in laminated composites: a review", *Composite Engineering*, Vol. 1, pp. 337-53.

Adolfsson, E. and Gudmundson, P. (1997), "Thermoelastic properties in combined bending and extension of thin composite laminates with transverse matrix cracks", *International Journal of Solids and Structures*, Vol. 34, pp. 2035-60.

Adolfsson, E. and Gudmundson, P. (1999), "Matrix crack initiation and progression in composite laminates subjected to bending and extension", *International Journal of Solids and Structures*, Vol. 36, pp. 3131-69.

Aveston, J. and Kelly, A. (1973), "Theory of multiple fracture of fibrous composite", *Journal of Materials Science*, Vol. 8, pp. 352-62.

Caiazzo, A.A. and Costanzo, F. (2001), "Modeling the constitutive behavior of layered composite with evolving cracks", *International Journal of Solids and Structures*, Vol. 38, pp. 3469-85.

Caiazzo, A.A. and Costanzo, F. (2002), "On the constitutive relation of materials with evolving microstructure due to micro-cracking", *International Journal of Solids and Structures*, Vol. 37, pp. 3375-98.

Chang, C.C., Chang, T.Y.P. and Xu, Y.G. (2000), "Structural damage detection using an iterative neural network", *Journal of Intelligent Material Systems and Structures*, Vol. 11, pp. 32-42.

Choi, C.T., Wu, H.Y.T. and Chang, F.K. (1991a), "A new approach towards understanding damage mechanics and mechanics of laminated composites due to low-velocity impact. Part I – Experiments", *Journal of Computers and Materials*, Vol. 25, pp. 992-1011.

Choi, C.T., Wu, H.Y.T. and Chang, F.K. (1991b), "A new approach towards understanding damage mechanics and mechanics of laminated composites due to low-velocity impact. Part II – Analysis", *Journal of Computers and Materials*, Vol. 25, pp. 1012-38.

Darmala, T.R., Karpur, P. and Bhagat, P.K. (1992), "A self learning neural net for ultrasonic signal analysis", *Ultrasonics*, Vol. 10 No. 3, pp. 317-24.

Doebling, S.W., Farrar, C.R., Prime, M.B. and Shevitz, D.W. (1996), "Damage identification and health monitoring of structural and mechanical systems from changes in their vibration characteristics: a literature review", Report, La-13070-MS, Los Alamos National Laboratory.

Doyle, J.F. (1997), *Wave Propagation in Structures*, Springer Verlag, New York, NY.

Frantziskonis, G. and Desai, C.S. (1991), "Surface degradation mechanisms in brittle material structural systems", *International Journal of Fracture*, Vol. 48, pp. 231-44.

Frantziskonis, G. and Joshi, S.P. (1990), "Damage evolution and constitutive behavior of advanced composites", *Composite Structures*, Vol. 16, pp. 341-57.

Friedman, J.H. (1987), "Exploratory projection pursuit", *Journal of the American Statistical Association*, Vol. 82 No. 397, pp. 249-66.

Garg, A.K., Roy Mahapatra, D., Suresh, S., Gopalakrishnan, S. and Omkar, S. (2004), "Estimation of composite damage model parameters using spectral finite element and neural network", *Composite Science and Technology*.

Gerald, C. (2000), "Modelling of the mechanical behaviour and damage processes of fibrous ceramic matrix composites: application to a 2-D SiC/SiC", *International Journal of Solids and Structures*, Vol. 37, pp. 919-42.

Hackett, R.M. and Kerry, T.S. (1992), "Modelling stiffness degradation in filamentary composite materials", *Journal of Materials in Civil Engineering*, Vol. 4 No. 2, pp. 196-211.

Hahn, H.T. and Tsai, S.W. (1974), "On the behavior of composite laminates after initial failures", *Journal of Composite Materials*, Vol. 8, pp. 288-305.

Han, Y.M. and Hahn, H.T. (1989), "Ply cracking and property degradations of symmetric balanced laminates under general in-plane loading", *Composites Science and Technology*, Vol. 35, pp. 377-97.

Harman, H.H. (1967), *Modern Factor Analysis*, 2nd ed., University of Chicago Press, Chicago, IL.

Haykins, S. (2001), *Neural Networks*, Pearson Education Inc., Harlow.

Hyvarinen, A. (1990), "Fast and robust fixed-point algorithms for independent component analysis", *IEEE Transactions on Neural Networks*, Vol. 10 No. 3, pp. 626-34.

Hyvarinen, A. (1999), "Survey on independent component analysis", *Neural Computing Surveys*, Vol. 2, pp. 94-128.

Ishak, S.I., Liu, G.R., Shang, H.M. and Lim, S.P. (2001), "Locating and sizing of delamination in composite laminates using computational and experimental methods", *Composites: B*, Vol. 32, pp. 287-98.

Joshi, S.P. and Frantziskonis, G. (1991), "Damage evolution in laminated advanced composites", *Composite Structures*, Vol. 17, pp. 127-39.

Kashtalyan, M. and Soutis, C. (2000), "Stiffness degradation in cross-ply laminates damaged by transverse cracking and splitting", *Composites: A*, Vol. 31, pp. 335-51.

Kumar, D.S., Roy Mahapatra, D. and Gopalakrishnan, S. (2003), "A spectral finite element for wave propagation and structural diagnostic analysis of composite beam with transverse crack", *Finite Elements in Analysis and Design*.

Liu, G.R. and Achenbach, J.D. (1995), "Strip element method to analyze wave scattering by cracks in anisotropic laminated plates", *Journal of Applied Mechanics*, Vol. 62, pp. 607-13.

Liu, S., Kutlu, Z. and Chang, F.K. (1993), "Matrix cracking and delamination in laminated composite beams subjected to a transverse concentrated line load", *Journal of Computers and Materials*, Vol. 27, pp. 436-70.

Liu, S.W., Huang, J.H., Sung, J.C. and Lee, C.C. (2002), "Detection of cracks using neural networks and computational mechanics", *Computational Methods in Applied Mechanical Engineering*, Vol. 191, pp. 2831-45.

Luo-Yu, X. (1994), "Interaction between matrix cracking and edge delamination in composite materials", *Composite Science and Technology*, Vol. 50, pp. 469-78.

Luo-Yu, X. (1996), "Study on the characteristics curve of stiffness degradation caused by transverse matrix cracking in multi-directional composite laminate", *Journal of Composite Materials*, Vol. 30 No. 7, pp. 820-38.

Manson, G., Worden, K. and Allman, D. (2003), "Experimental validation of a structural health monitoring methodology. Part I. Novelty detection on a laboratory structure", *Journal of Sound and Vibration*, Vol. 259 No. 2, pp. 345-63.

Nag, A., Roy Mahapatra, D. and Gopalakrishnan, S. (2002a), "Identification of delaminations in composite beams using spectral estimation and genetic algorithm", *Smart Materials and Structures*, Vol. 11, pp. 105-26.

Nag, A., Roy Mahapatra, D. and Gopalakrishnan, S. (2002b), "Identification of delaminations in a composite beam using a damaged spectral element", *Structural Health Monitoring*, Vol. 1 No. 1, pp. 105-26.

Nag, A., Roy Mahapatra, D., Gopalakrishnan, S. and Sankar, T.S. (2003), "A spectral finite element with embedded delamination for modeling of wave scattering in composite beams", *Composite Science and Technology*.

Ogihara, S. and Takeda, N. (1995), "Interaction between transverse cracks and de-lamination during damage progress in CFRP cross-ply laminates", *Composite Science and Technology*, Vol. 54, pp. 395-404.

Oja, E. (1982), "A simplified neuron model as a principal component analyzer", *Journal of Mathematical Biology*, Vol. 15, pp. 267-73.

Oja, E. and Hyvarinen, A. (2004), *Independent Component Analysis: A Tutorial*, Helsinki University of Technology, Helsinki.

Olshausen, B.A. and Field, D.J. (1996), "Emergence of simple-cell receptive field properties by learning a sparse code for natural images", *Nature*, Vol. 381, pp. 607-9.

Olshausen, B.A. and Field, D.J. (1997), "Sparse coding with an overcomplete basis set: a strategy employed by V1", *Vision Research*, Vol. 37, pp. 3311-25.

Ratcliffe, C.P. (2000), "A frequency and curvature based experimental method for locating damage in structures", *Journal of Vibration and Acoustics*, Vol. 122 No. 3, pp. 324-9.

Rhim, J. and Lee, S.W. (1995), "A neural network approach for damage detection and identification of structures", *Computational Mechanics*, Vol. 16, pp. 437-43.

Roy Mahapatra, D. and Gopalakrishnan, S. (2003), "A spectral finite element model for analysis of axial-flexural-shear coupled wave propagation in laminated composite beams", *Composite Structures*, Vol. 59 No. 1, pp. 67-88.

Schulz, M.J., Naser, A.S., Pai, P.F. and Chung, J. (1998), "Locating structural damage using frequency response reference functions", *Journal of Intelligent Material Systems and Structures*, Vol. 9, pp. 899-905.

Song, S.J. and Schmerr, L.W. (1992), "Ultrasonic flow classification in weldments using probabilistic neural networks", *Journal of Non Destructive Evaluation*, Vol. 11 No. 2, pp. 69-77.

Sung, D-U., Jung-Hoon, O., Kim, C-G. and Hong, C-S. (2000), "Impact monitoring of smart composite laminates using neural network and wavelet analysis", *Journal of Intelligent Material Systems and Structures*, Vol. 11, pp. 180-90.

Suresh, S., Omkar, S.N., Mani, V. and Guru Prakash, T.N. (2003), "Lift coefficient prediction at high angle of attack using recurrent neural network", *Aerospace Science and Technology*, Vol. 7, pp. 595-602.

Toyama, N., Noda, J. and Okabe, T. (2003), "Quantitative damage detection in cross-ply laminates using Lamb wave method", *Composite Science and Technology*, Vol. 63, pp. 1473-9.

Wu, X., Ghaboussi, J. and Garett, J.H. (1992), "Use of neural networks in detection of structural damage", *Computers and Structures*, Vol. 42 No. 4, pp. 649-59.

Xu, Y.G. and Liu, G.R. (2002), "Detection of flaws in composites from scattered elastic-wave field using an improved μGA and a local optimizer", *Computer Methods in Applied Mechanics and Engineering*, Vol. 191, pp. 3929-46.

Zgonc, K. and Achenbach, J.D. (1996), "A neural network for crack sizing trained by finite element calculations", *Non Destructive Testing and Evaluation Int.*, Vol. 29 No. 3, pp. 147-55.

Zhang, J. and Herrmann, K.P. (1999), "Stiffness degradation induced by multilayer intra-laminar cracking in composite laminates", *Composites: A*, Vol. 30, pp. 683-706.

Zhang, H., Schulz, M.J., Naser, A., Ferguson, F. and Pai, P.F. (1999), "Structural health monitoring using transmittance functions", *Mechanical Systems and Signal Processing*, Vol. 13 No. 5, pp. 765-87.